

Vestiges of Underplating and Assemble in the Central North China Craton Based on Noise Tomography

Chuansong He¹ and Haoyu Tian²

¹Institute of Geophysics China Earthquake Administration

²Institute of Geophysics, CEA

November 22, 2022

Abstract

The study region is located in the central part of the North China craton (NCC). We use one-year continuous waveforms of the vertical component from 112 broadband seismic stations and obtain the group velocity dispersion curves of Rayleigh waves for different periods through single station data preprocessing, cross-correlation calculation, stacking, group velocity dispersion measurement and quality evaluation. We then use the surface wave tomography method to obtain the Rayleigh wave group velocity distributions at 9-40 s in this area. Finally, the S-wave velocity structures at depths of 0-60 km are determined by pure path dispersion inversion. The results show that the crustal structure of the Eastern Block is different from those of the Western Block and the Trans-North China orogen. The lower crust of the Eastern Block shows a high-velocity S-wave anomaly, which may be related to magma underplating in the lower crust induced by an upwelling mantle plume. From the surface to the top of the mantle, the S-wave velocity of the Western Block decreases gradually, and the crust of the Trans-North China orogen shows a relatively high S-wave velocity. The results characterize the S-wave velocity structures of the different geological units and have important scientific significance for understanding the destruction of the NCC.

Hosted file

essoar.10507384.1.docx available at <https://authorea.com/users/530576/articles/597888-vestiges-of-underplating-and-assemble-in-the-central-north-china-craton-based-on-noise-tomography>

Vestiges of Underplating and Assemble in the Central North China Craton Based on Noise Tomography

Haoyu Tian, Chuansong He¹

(Institute of Geophysics, China Earthquake Administration, Beijing 100081, China)

Abstract: The study region is located in the central part of the North China craton (NCC). We use one-year continuous waveforms of the vertical component from 112 broadband seismic stations and obtain the group velocity dispersion curves of Rayleigh waves for different periods through single station data preprocessing, cross-correlation calculation, stacking, group velocity dispersion measurement and quality evaluation. We then use the surface wave tomography method to obtain the Rayleigh wave group velocity distributions at 9-40 s in this area. Finally, the S-wave velocity structures at depths of 0-60 km are determined by pure path dispersion inversion. The results show that the crustal structure of the Eastern Block is different from those of the Western Block and the Trans-North China orogen. The lower crust of the Eastern Block shows a high-velocity S-wave anomaly, which may be related to magma underplating in the lower crust induced by an upwelling mantle plume. From the surface to the top of the mantle, the S-wave velocity of the Western Block decreases gradually, and the crust of the Trans-North China orogen shows a relatively high S-wave velocity. The results characterize the S-wave velocity structures of the different geological units and have important scientific significance for understanding the destruction of the NCC.

Key words: Noise tomography, Rayleigh wave velocity, S-wave velocity, Crustal structure, Destruction of the North China craton, Trans-North China orogen.

Plain Language summary:

We carried out noise tomography in the central part of the North China craton (NCC) and obtained the Rayleigh wave group velocity distributions at 9-40 s as well as the S-wave velocity structures at depths of 0-60 km. The results show that the lower crust of the Eastern Block shows a high-velocity S-wave anomaly, which may be related to magma underplating in the lower crust induced by an upwelling mantle plume. From the surface to the top of the mantle, the crust of the Trans-North China orogen shows a relatively high S-wave velocity, which imply a vestige of the collision and assemble between the Eastern and Western Craton, whereas the S-wave velocity of the Western Block decreases gradually. The results characterize the S-wave velocity structures of the different geological units and have important scientific significance for understanding the destruction of the NCC.

1. Introduction

The North China craton (NCC) is one of the world's oldest cratons (Zheng et

¹* Corresponding author. hechuansong@aliyun.com (C.S.H)

al., 2004). The NCC consists of two Precambrian terranes, the Eastern Craton (or Block) and the Western Craton (or Block) (Fig. 1). In the Paleoproterozoic, they assembled together along the Trans-North China orogen (Zhao et al., 2005). From the Paleoproterozoic to the late Cambrian, the NCC remained stable for several hundred Ma (Yang and Santosh, 2017). Since the Mesozoic, the region has experienced multiple periods of collision among terranes and the subduction of the Pacific plate, and the craton structure has been largely destroyed (Ren, 1991). There are different models for the mechanism of craton destruction, such as thermal erosion generated by mantle upwelling (e.g., Zheng et al., 1998; Menzies et al., 1993) and lower crustal/lithospheric delamination induced by the north-south amalgamation of terranes (e.g., Gao et al., 1998; He, 2020).

To reveal evidence of deep structures associated with craton destruction, many geophysical works have been carried out in this region (e.g., Pandey, et al., 2014; Pei et al., 2006; Zhang et al., 2019; He, 2015, 2020; Lei, 2012). In particular, He et al. (2015) detected a region with high V_p/V_s ratios in the Eastern Block that may be connected with magma underplating induced by mantle plume upwelling. Lei (2012) and He (2020) revealed a vestige of Mesozoic mantle plume upwelling based on teleseismic P-wave tomography beneath the Eastern Block. However, whether this represents a relic or evidence of magma underplating in the crust remains unclear. On the other hand, the difference in the velocity structures among the Eastern Block, Western Block and Trans-North China orogen is still vague, although it is very important for understanding the destruction of the NCC and the assembly between the Eastern Block and Western Block.

In this study, we carried out noise tomography in the middle part of the NCC. The results show that there are great differences in the S-wave velocity structure among the Western Block, Eastern Block and Trans-North China orogen. We also reveal a distinctive velocity anomaly in the lower crust beneath the Eastern Block, which might be associated with magma underplating.

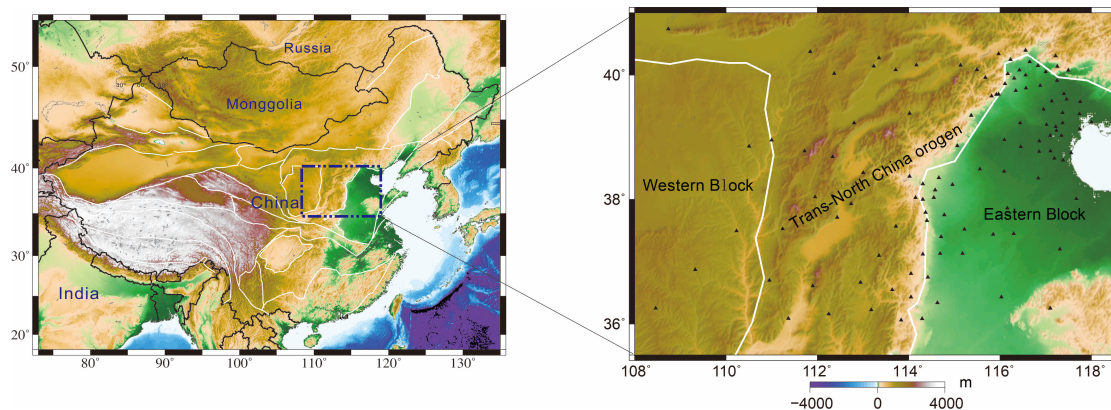


Fig. 1. Left panel: location of the study region. Right panel: distribution of seismic stations. The thick white lines are the boundaries of geological units. The black triangles indicate the seismic stations. The study area is located in

the central part of the NCC, which is the suture zone between the Eastern and Western Blocks.

1. Data and method

(a) Data and processing

Based on a direct cross-correlation of the continuous background noise between two stations, we can obtain high-resolution seismic imaging in the crust and upper mantle (Lobkis and Weaver, 2001; Campillo and Paul, 2003; Shapiro et al., 2005; Yao et al., 2006; Bensen et al., 2007; Fang et al., 2010). Noise tomography has advanced our seismic imaging techniques (Lu et al., 2014).

In this study, the continuous waveforms of the vertical component recorded by 112 stations from January 2018 to December 2018 were collected from the Data Management Center of the China National Seismic Network (Zheng et al., 2010). Based on the method of Bensen et al. (2007), we resampled the continuous waveforms to 5 Hz and cut the data from 0 to 24 hours. Other steps involved clock synchronization, instrument response removal, bandpass filtering (4–50 s period), time-domain normalization and spectral whitening. Finally, the day-long waveform at each station was correlated with those at other seismic stations, and the daily results at each station were stacked to produce the final cross-correlation results.

The surface wave signals coming from opposite directions along the path linking the stations can be inferred from the resulting cross-correlations. Due to the inhomogeneous distribution of ambient noise sources, the cross-correlations might be asymmetrical. To enhance the signal-to-noise ratio of the surface waves and simplify data analysis, each cross-correlation can be separated into negative and positive lag components, and then the two components can be added to form the so-called symmetric component. The following analysis was performed exclusively on the symmetric signals.

Based on multiple filtering technologies (Dziewonski et al., 1969; Levshin et al., 1992), we manually pick the group velocity dispersion curve with Computer Programs in Seismology (CPS) software (Herrmann, 1973). If there are n stations, we can extract empirical Green’s functions on $n(n-1)/2$ paths. To ensure reliable results, we perform quality control of the dispersion curve.

If the interstation distance is at least 3 times the wavelength at a given period and its signal-to-noise ratio is greater than 10, an empirical Green’s function can be accepted (Yao et al., 2006; Bensen et al., 2007). Accordingly, paths are shorter than 120 km are excluded. Finally, we select a total of 1774 dispersion curves for the station pairs from the 6216 Rayleigh wave waveform data (example, see Fig. 2). In Fig. 3, we show the number of ray paths used for surface wave imaging at different periods, which indicates that the number of rays at different periods is relatively uniform.

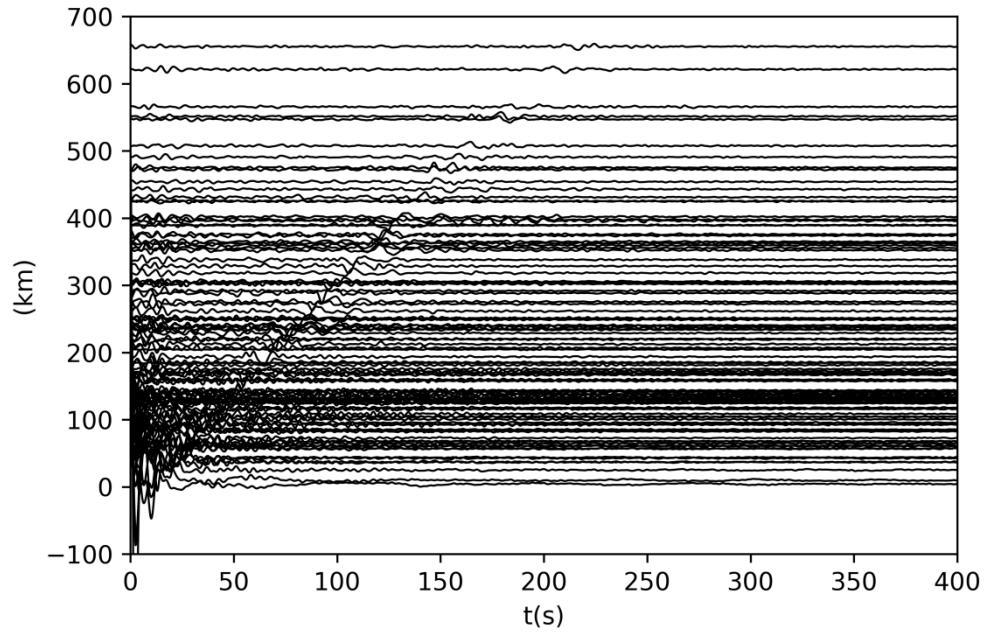


Fig. 2. Example of the correlation of one-year data from the ZKD seismic station related to other seismic stations with periods from 5 to 50 s.

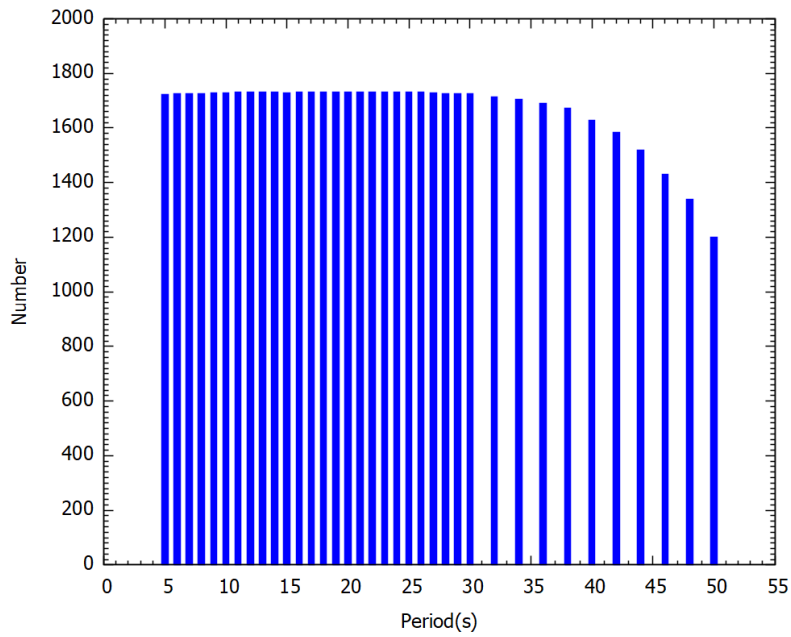


Fig. 3. The number of group velocity dispersion curves at different periods.

1. Rayleigh wave velocity and S-wave velocity inversion

In the process of surface wave tomography, a generalized 2-D linear inversion procedure is used to construct the distribution of the group velocity (Yanovskaya and Ditmar, 1990; Ditmar and Yanovskaya, 1987), which is a generalization to 2-D inferred from the classic 1-D method of Backus and Gilbert (1968). In the inversion process, a $0.5^\circ \times 0.5^\circ$ lateral grid is designed, and a value of $\gamma = 0.2$ (damping parameter) is selected, which controls the tradeoff between the fit to the data and the smoothness of the resulting group velocity maps and yields relatively smooth maps with small fit errors.

From the Rayleigh wave group velocity obtained by the above inversion approach, the dispersion curves of the group velocity at each grid node are extracted. The 1-D shear wave velocity structure under each grid node is then inverted (Herrmann and Ammon, 2004), and the velocities between the nodes are interpolated linearly. In this way, we construct a 3-D shear wave velocity structure (Fig. 4).

A constant shear-wave velocity of 4.38 km/s from the surface to a depth of 90 km is designed for the initial model, which is divided into 2 km layers. Because the starting velocity model is overestimated, no artificial low-velocity zone or layer boundary is introduced as a consequence of the nonlinearity of the inversion. In the inversion process, a fixed V_p/V_s ratio of 1.732 is adopted, and the density is obtained from the P-wave velocity (Zanjani et al., 2019).

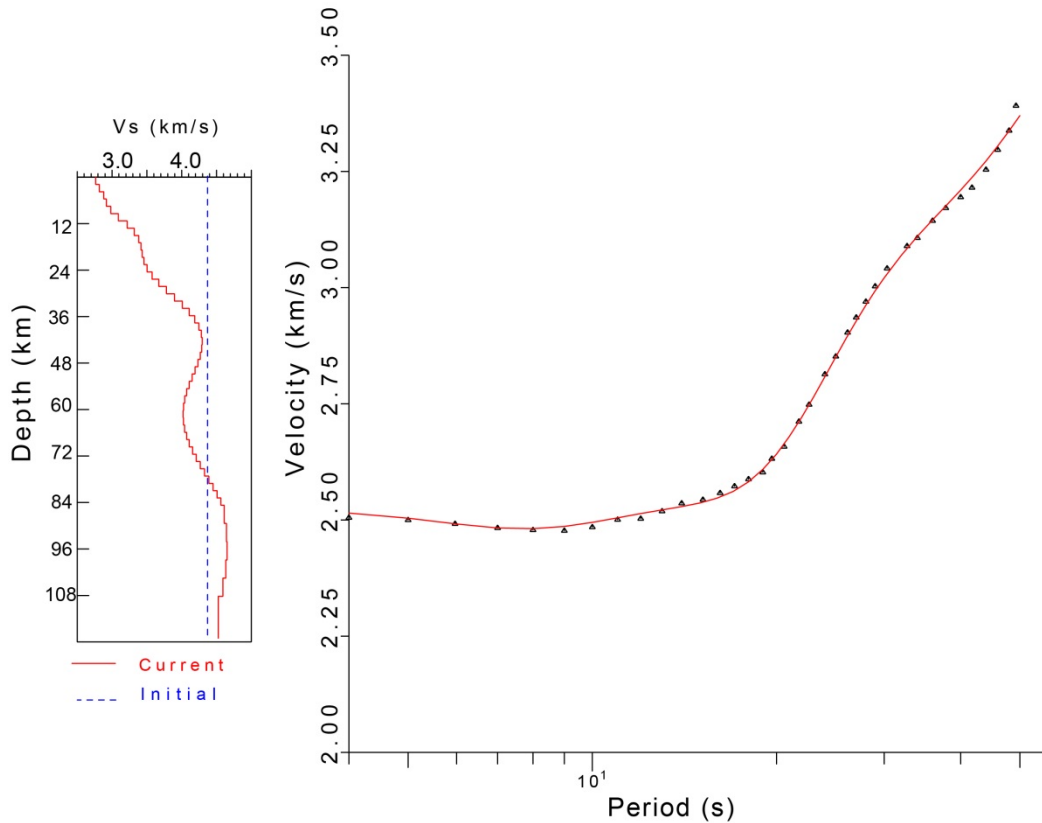


Fig. 4. An example to illustrate the process of inverting the S-wave velocity from the dispersion curve at a node (116.5°E, 38°N). The red solid line represents the theoretical group velocity dispersion generated by the final S-wave velocity model and obtained from the inversion. The black triangles in the right panel indicate the dispersion of group velocity observations. The blue dashed line in the left panel represents the initial velocity model, whereas the red solid line represents the final S-wave velocity model obtained by the inversion.

1. Resolution analysis and results

(a) Resolution analysis

Generally, the checkerboard resolution test (CRT) is used to analyze the resolution and estimate the error of the results. However, Leveque et al. (1993) considered that the CRT used to analyze resolution may lead to errors. Yanovskaya (1997, 1998) used the mean scale and the stretch of the mean area to estimate the imaging resolution, and the resolution of tomographic results was calculated based on the ray density and the ray azimuth distribution.

Fig. 5 represents the resolution of each period. The resolution radius distribution shows that the minimum resolution radius can reach 50 km, whereas

for most research areas, the resolution core radius can reach 200 km. In this region, the obtained spatial average resolution radius is between 0 and 200 km, and the resolution radius is completely within the smooth radius allowed by the model parameters. According to the results of the resolution detection, we consider that the inversion results for most areas in our study region are relatively reliable.

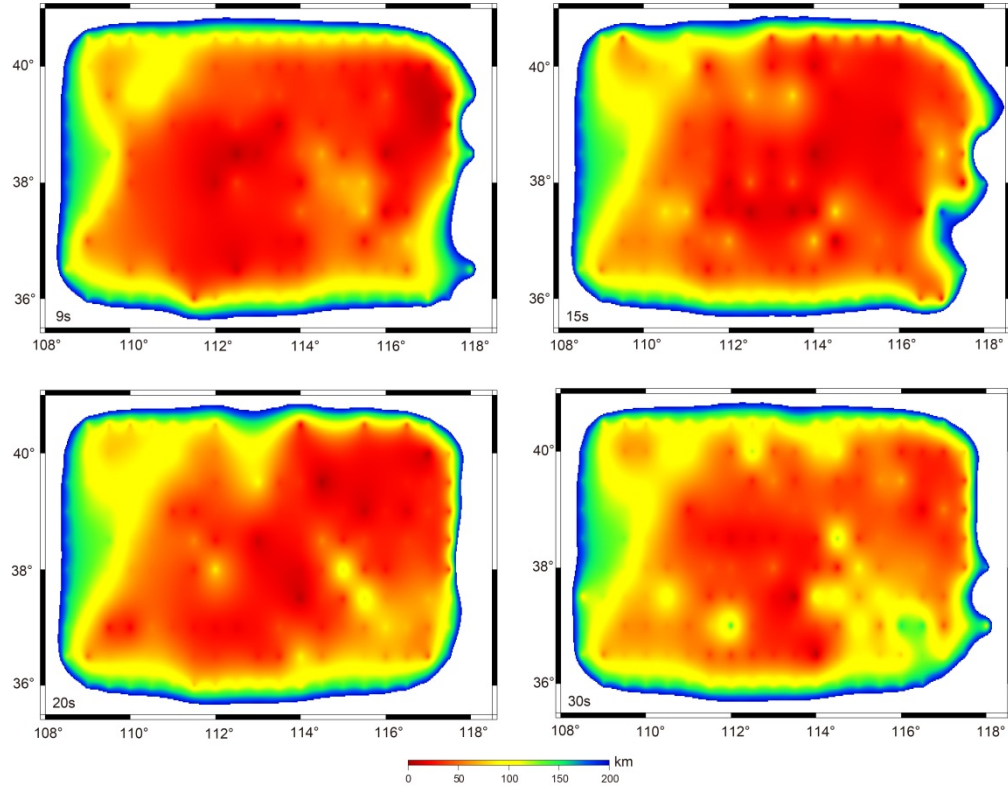


Fig. 5. The distribution of the spatial average resolution radius at different periods. The color scale at the bottom shows the value of the resolution radius.

1. Rayleigh wave velocity

Because the group velocities at different periods have different sensitivities to the shear wave velocity in different depth ranges (Urban et al., 1993), it is necessary to take the partial derivatives of the group velocities of different periods and obtain the sensitivity kernels of the fundamental Rayleigh wave. Our results show that the group velocity at a 38 s period has a good resolution from 30 km to 45 km (Fig. 6), which is our target region.

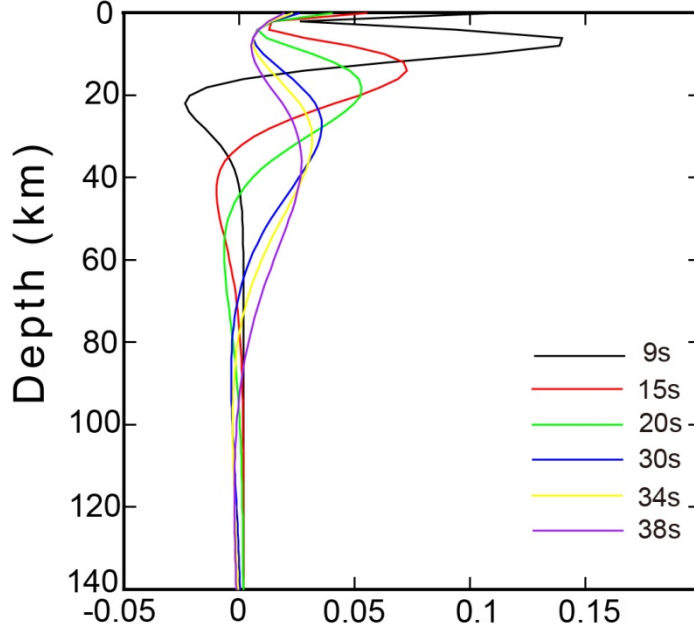


Fig. 6. Sensitivity kernels of fundamental Rayleigh group velocities at 9 s, 15 s, 20 s, 30 s, 34 s and 38 s. The AK135 model is adopted for calculation, and the crust thickness is set at 36 km.

The group velocity of a certain period is most sensitive to the shear wave velocity of $1/3$ wavelength (Lin et al., 2007; Yang et al., 2007), and the structural differences at different depths lead to variations in the group velocity. Here, the representative group velocities of the six periods are discussed (Fig. 7). The velocity distribution image of the Rayleigh wave group at $T=9$ s mainly reflects the velocity structure of the upper crust. The velocities of the Rayleigh wave groups at $T=15$ s and 20 s mainly reflect the velocity structure of the middle crust. The velocities of the Rayleigh wave groups at medium and long periods (30-38 s) mainly reflect the velocity structure from the lower crust to the top of the mantle (Fig. 7).

The results show that the group velocities at 9 s-38 s in the Trans-North China orogen are higher than those of the terranes on either side (Eastern and Western Blocks). The group velocity from the surface to the top of the mantle in the Western Block decreases gradually. The Eastern Block has a low-velocity structure at a period of 9 s, which may be affected by the sedimentary layer near the surface; this block also has a low-velocity structure from 15 s to 30 s, which may include the sedimentary effect and the low-velocity anomaly in the middle crust. At 34-38 s, it has a high-velocity structure, which represents the region from the lower crust to the top of the upper mantle.

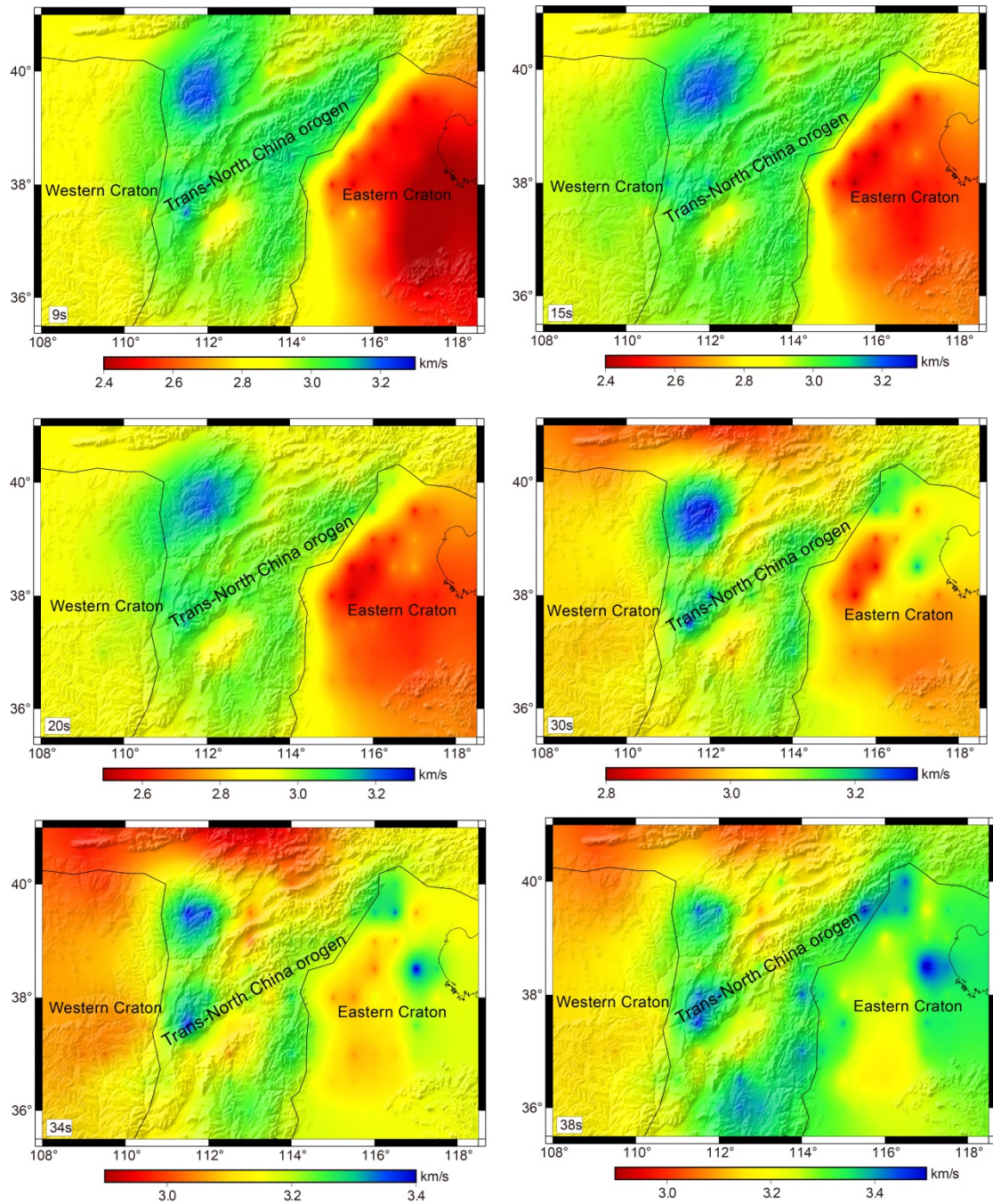


Fig. 7. Rayleigh wave group velocities at the different periods. Western Block (or Craton). Eastern Block (or Craton).

3.3. S-wave velocity structure

Based on the 1-D shear wave velocity structure of each grid node obtained in this study, we can construct a 3-D shear wave velocity structure ranging from a depth of 6 km to a depth of 42 km in this area (Fig. 8). The results show that the S-wave velocity of the Trans-North China orogen is higher than those of the Eastern and Western Blocks from the surface to the top of the mantle, which is consistent with the group velocity (Fig. 7, Fig. 8). In the Western Block, the S-wave velocity decreases gradually from the surface to the top of the mantle, which is basically consistent with the group velocity (Fig. 7, Fig. 8). In the Eastern Block, a low-velocity structure of the S-wave is observed at a depth of 6 km, a low-velocity structure is noted at depths of 10-20 km, and a high-velocity structure is detected at depths of 38-42 km, which is basically consistent with the group velocity results (Fig. 7, Fig. 8).

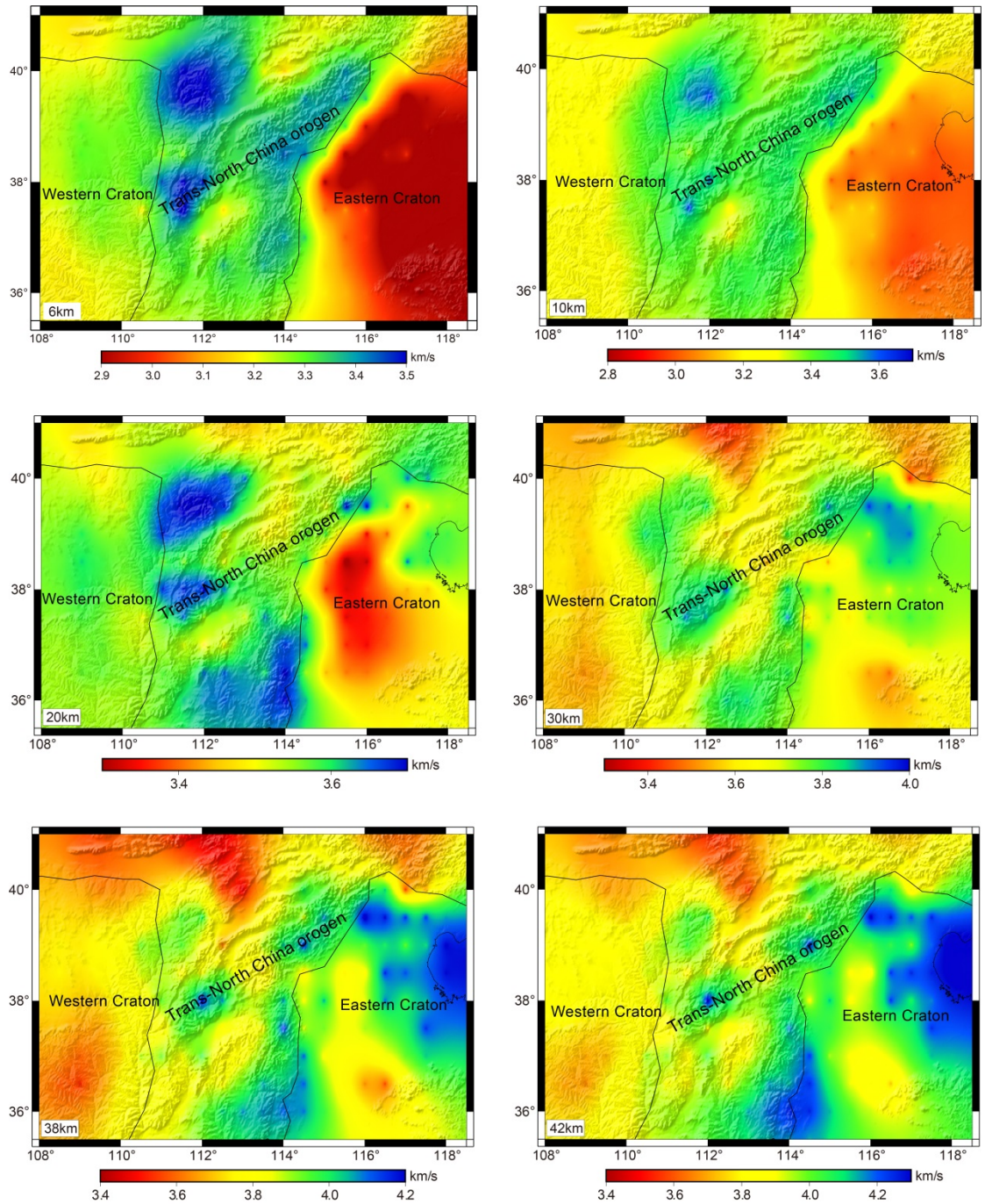


Fig. 8. S-wave velocity at depths of 6 km, 10 km, 20 km, 30 km, 38 km and 42 km. Western Block (or Craton). Eastern Block (or Craton).

1. Discussion

He et al. (2015) obtained a V_p/V_s distribution image of the NCC by using the H-k technique for stacking of receiver functions. The results showed a region with high V_p/V_s ratios ($V_p/V_s > 1.76$, red ellipse) in the northern NCC (Fig. 9, red ellipse region). In general, magma underplating in the lower crust can lead to high V_p/V_s ratios (Zandt and Amgon, 1995; Xu and He, 2007) and high-velocity anomalies in the lower crust (Zandt and Amgon, 1995). This study reveals that the lower crust in the Eastern Block has a high-velocity anomaly in the lower crust, which further indicates that a deep process of magma underplating occurs in this area. Due to the uneven distribution of seismic stations in the Eastern Block (Fig. 9, black triangles), the region with high V_p/V_s ratios in the Eastern Block is not completely controlled. However, there are still considerable areas corresponding to the high-velocity structure in the lower crust. On the other hand, we consider that the low-velocity anomaly at a depth of 20 km may be associated with a magma intrusion induced by mantle plume upwelling, although we cannot exclude that this anomaly may be affected by the sedimentary layer.

In general, an upwelling mantle plume plays a key role in magma intrusion and lower crust underplating (Pirajno, 2007). He (2020) revealed a mushroom-like low-velocity structure beneath the Eastern Block by using P-wave teleseismic tomography; such a structure is a typical characteristic of mantle plume upwelling (Fig. 10). Therefore, we suggest that the low-velocity anomaly in the middle crust revealed beneath the Eastern Block may be generated by mantle plume upwelling and magma intrusion.

Although He et al. (2015) also revealed a region with high V_p/V_s ratios in the Western Block (Fig. 9, green ellipse region), we have confirmed that the lower crust has a low-velocity structure, which rules out the occurrence of a deep process of magma underplating in the lower crust in this region.

Both group velocities and S-wave velocities indicate that the Trans-North China orogen is a high-velocity structural terrane, which is quite different from the Eastern Block and Western Block. This contrast indicates that the Trans-North China orogen is an independent geological unit that connects the Eastern and Western Blocks of the craton and may represent the vestige of collision and assembly in the Paleoproterozoic.

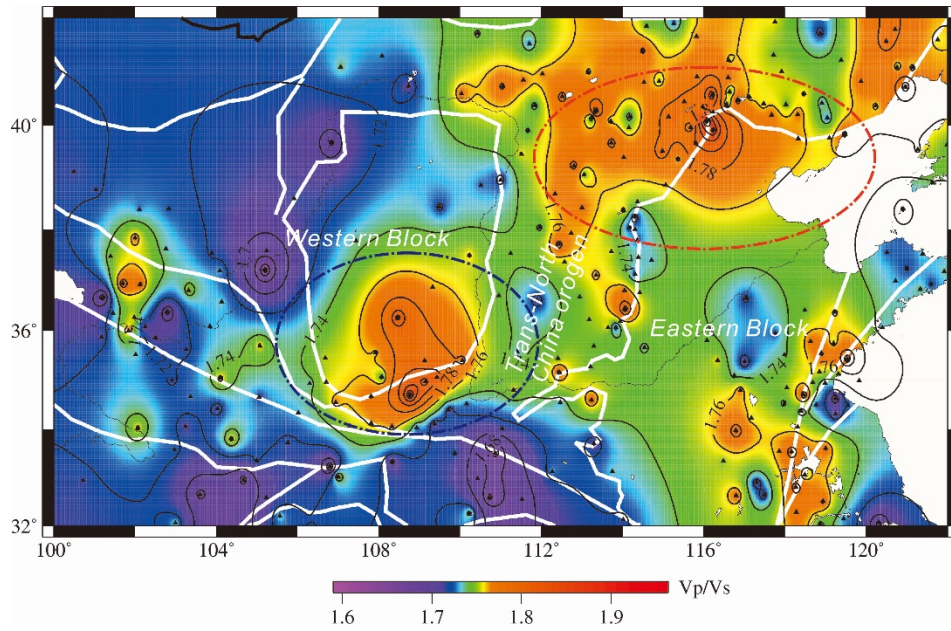


Fig. 9. V_p/V_s ratio distribution in the NCC (He et al., 2015). Black triangles mark seismic stations.

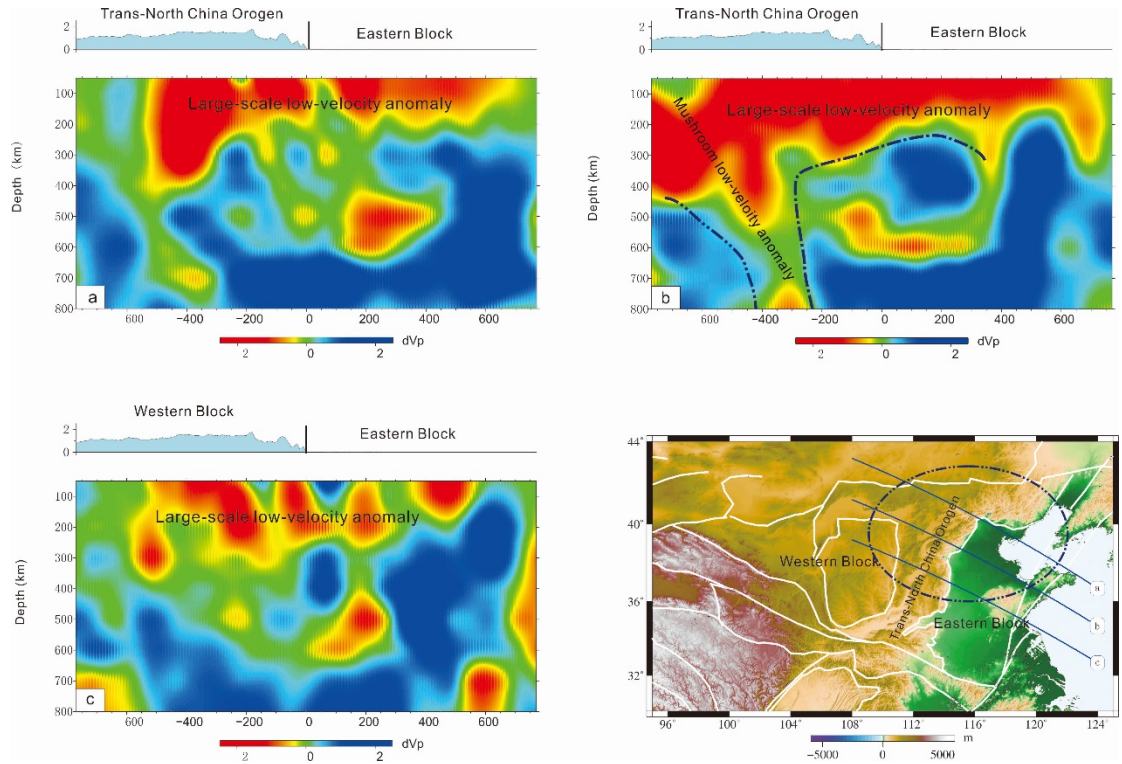


Fig. 10. P-wave velocity perturbation profile (He, 2020), b: Low-velocity anomaly with a mushroom shape.

5. Conclusions

This study reveals that the group velocities and S-wave velocities of the Eastern and Western Blocks as well as the Trans-North China orogen are quite different. The high V_p/V_s in the Western Block may represent the ancient lower crust, which has not been destroyed, while the high V_p/V_s in the Eastern Block may reflect magma underplating in the lower crust induced by mantle plume upwelling, which implies that mantle plume upwelling may have contributed to the destruction of the Eastern Block of the NCC. On the other hand, we also suggest that the Trans-North China orogen represents the assembly or collision between the Western Block and Eastern Block in the Paleoproterozoic.

Acknowledgments

We thank the National Key R&D Plan of China (2017YFC601406). Waveform data for this study were provided by the Data Management Center of the China National Seismic Network at the Institute of Geophysics (Zheng et al., 2010). The cross-correlation function involved in the noise tomography can be accessed via <https://doi.org/10.5281/zenodo.4971734>.

References

- Bensen, G. D., Ritzwoller, M. H., & Bamin, M. P. (2007). Processing seismic ambient noise data to obtain reliable broad-band surface wave dispersion measurements. *Geophysical Journal International*, *169*(3), 1239-1260.
- Backus, G., & Gilbert, F. (1968). Resolving power of gross earth data. *Geophys J R Astron Soc*, *16*, 169-205.
- Backus, G. E., & Gilbert, F. (1968). The resolving power of gross Earth data. *Geophysical Journal International*, *16*, 169-205.
- Campillo, M., & Paul, A. (2003), Long-Range correlations in the diffuse seismic coda. *Science*, *299*, 547-549, doi: 10.1126/science.1078551.
- Ditmar, P. G. & Yanovskaya, T. B., (1987). A generalization of the Backus-Gilbert method for estimation of lateral variations of surface wave velocity. *Izv Akad Nauk SSSR Fiz Zeml in Russian* *6*, 30-60.
- Dziewonski, A., (1969). A technique for the analysis of transient seismic signals. *Bulletin of the Seismological Society of America* *59*, 427-444.
- Fang, L., Wu, J., & Ding, Z., (2010). High resolution Rayleigh wave group velocity tomography in North China from ambient seismic noise. *Geophysical Journal International*, *181*(2), 1171-1182.
- He, C. S., Dong, S. W., Santosh, M., Li, Q., & Chen, X., (2015). Destruction of the north China Craton: a perspective based on receiver function analysis. *Geological Journal*, *50*, 93-103.
- He, C. S., (2020). Upwelling mantle plume and lithospheric delamination beneath the North China Craton. *Physics of the Earth and Planetary Interiors*, *306*, 106548.
- Herrmann, R. B., & Ammon, C. J., (2004). Surface waves, receiver functions, and crustal structure. *Computer Programs in Seismology, Version 3.30*.
- Herrmann, R. B., (1973). Some aspects of band-pass filtering of surface waves. *Bulletin of the Seismological Society of America*, *63*(2), 663-671.
- Gao, S., Zhang, B. R., Jin, Z. M., Kern, H., Luo, T. C., & Zhao, Z. D., (1998). How mafic is the lower continental crust?. *Earth and Planetary Science Letters*, *161*, 101-117.
- Lei, J., (2012). Upper-mantle tomography and dynamics beneath the North China Craton. *J. Geophys. Res.* *117*, B06313.
- Levshin, A., Ratnikova, L., & Berger, J., (1992). Peculiarities of surface-wave propagation across central Eurasia. *Bulletin of the Seismological Society of America*, *82*(6), 2464-2493.
- Leveque, J. J., Rivera, L., & Wittlinger, G., (1993). On the use of the checkerboard test to assess the resolution of tomographic inversions. *Geophysical Journal International*, *115*, 313-318.

- Lin, F. C., Ritzwoller, M. H., Townend, J., Bannister, S., & Savage, M. K., (2007). Ambient noise Rayleigh wave tomography of New Zealand. *Geophysical Journal International*, 170(2), 649-666.
- Lobkis, O. I. & Weaver, R. L., (2001). On the emergence of the green's function of in the correlations of a diffuse field. *Acoustical Society of America*, 110(6) 3011-3017.
- Lu, L. Y., He, Z., Ding, Z., & Wang, C., (2014). Azimuth anisotropy and velocity heterogeneity of Yunnan area based on seismic ambient noise. *Chinese Journal of Geophysics*, 57(3), 822-836.
- Menzies, M. A., Fan, W. M., & Zhang, M., (1993). Palaeozoic and Cenozoic lithoprobes and the loss of ~120 km of Archaean lithosphere, Sino-Korean craton, China. In: Magmatic processes and plate tectonics, Prichard, H.M., Alabaster, T., Harris, N.B.W., Neary, C.R. (eds.). Geological Society, London, Special Publications 76, 71-78.
- Pandey, S., Yuan, X., Debayle, E., Priestley, K., Kind, R., Tilmann, F., & Li, X., (2014). A 3-D shear-wave velocity model of the upper mantle beneath China and the surrounding areas. *Tectonophysics*, 633, 193-210.
- Pei, S., Zhao, J., Rowe, C. A., Charlotte, A. R., Wang, S. Y., Hearn, T. M., Xu, Z. H., Liu, H. B., & Sun, Y. S. (2006). ML Amplitude Tomography in North China. *Bull. Seismol. Soc. Am.*, 96, 1560-1566.
- Pirajno, F., (2007). Ancient to modern earth: the role of mantle plume in the making of continental crust: Earth's Oldest Rocks, edited by Kranendonk, M.J.V., Smithies, R.H., and Bennett, V.C., Developments in Precambrian Geology, v.15 (K.C. Condie, Series Editor), DOI: 10.1016/S0166-2635(07)15083-0.
- Ren, J., (1991). On the geotectonics of southern China. *Acta Geologica Sinica - English Edition*, 2, 111-136.
- Shapiro, N. M., Campillo, M., Stehly, L., & Ritzwoller, M. H., (2005). High resolution surface wave tomography from ambient seismic noise. *Science*, 307, 1615-1618, doi: 10.1126/science.1108339.
- Urban, L., Artur, C., & Franco, V., (1993). Computation of analytical partial derivatives of phase and group velocities for Rayleigh waves with respect to structural parameters. *Studia Geophysica et Geodaetica*, 37, 14-36.
- Weaver, R. L., & Lobkis, O. I., (2001). Ultrasonics without a Source: Thermal fluctuation correlation at MHz Frequencies. *Physical Review Letters*, 87(13) 134301.
- Xu, Y. G., & He, B., (2007). Thick and high velocity crust in Emeishan large igneous province, SW China: Evidence for crustal growth by magmatic underplating/intraplating. In: Foulger, G. and Jurdy, D. eds. The Origins of Melting Anomalies: Plates, Plumes, and Planetary Processes. *Geological Society of America Special Papers* 430, 841-858.

- Yang, Y., Ritzwoller, M. H., Levshin, A. L., & Shapiro, N. M., (2007). Ambient noise Rayleigh wave tomography across Europe. *Geophys. J. Int.*, 168, 259-274.
- Yang, Q., & Santosh, M., (2017). The building of an Archean microcontinent: Evidence from the North China Craton. *Gondwana Research* 50, 3-37.
- Yao, H., Van der Hilst, R. D. & de Hoop, M. V., (2006). Surface-wave array tomography in SE Tibet from ambient seismic noise and two-station analysis-I. Phase velocity maps. *Geophysical Journal International* 166 2 732 - 744.
- Yanovskaya, T. B., Ditmar, P. G., (1990). Smoothness criteria in surface-wave tomography. *Geophysical Journal International*, 102, 63-72.
- Yanovskaya, T. B., (1997). Resolution estimation in the problems of seismic ray tomography. *Izvestia, Physics of the Solid Earth*, 33(9), 762-765.
- Yanovskaya, T. B., Kizima, E. S., & Antonova, L. M., (1998). Structure of the Black Sea and adjoining regions from surface wave data. *J. Seismol.*, 2, 303-316.
- Zanjani, A. A., Zhu, L., & Herrmann, R. B., (2019). Crustal Structure beneath the Wabash Valley Seismic Zone from the Joint Inversion of Receiver Functions and Surface-Wave Dispersion: Implications for Continental Rifts and Intraplate Seismicity. *Journal of Geophysical Research: Solid Earth*, 124.
- Zandt, G., & Ammon, C. J., (1995). Continental crust composition constrained by measurements of crustal Poisson's ratio. *Nature*, 374(6518), 152-154.
- Zhao, G., Sun, M., Wilde, S. A., & Li, S., (2005). Late Archean to Paleoproterozoic evolution of the North China Craton: key issues revisited. *Precambrian Research*, 136, 177-202.
- Zhang, P., Yao, H., Chen, L., Fang, L., Wu, Y., & Feng, J., (2019). Moho depth variations from receiver function imaging in the northeastern North China Craton and its tectonic implications. *J. Geophys. Res.*, 124, 1852-1870.
- Zheng, J., Griffin, W. L., O'Reilly, S. Y., & Lu, F., (2004). 3.6 Ga lower crust in central China: new evidence on the assembly of the North China craton. *Geology*, 32, 229-232.
- Zheng, J. P., O'Reilly, S. Y., Griffin, W. L., Lu, F. X., & Zhang, M., (1998). Nature and evolution of Cenozoic lithospheric mantle beneath Shandong peninsula, Sino-Korean craton, eastern China. *International Geology Review*, 40, 471-499.
- Zheng, X., Yao, Z., Liang, J., Zheng, J., (2010). The role played and opportunities provided by IGP DMC of China National Seismic Network in Wenchuan earthquake disaster relief and researches. *Bulletin of the Seismological Society of America*, 100(5B), 2866-2872